International Journal of Network Dynamics and Intelligence Scilight

Article

Recursive Strong Tracking Filtering for Power Harmonic Detection With Outliers-Resistant Event-Triggered Mechanism

Xingzhen Bai [1,*], Guhui Li [1], Mingyu Ding [2], Liqun Yu [1], and Yufeng Sun [1]

[1] College of Electrical Engineering and Automation, Shandong University of Science and Technology, Shandong 266590, China
[2] State Grid Dong'e County Power Supply Company in Shandong Province, Dong'e, 252200, China
[*] Correspondence: xzbai@sdust.edu.cn

Received: 24 September 2023
Accepted: 25 December 2023
Published: 24 December 2024

Abstract: This paper is concerned with the problem of power harmonic detection subject to communication resource constraints and measurement outliers. A dynamic tracking model is established to capture the dynamics of harmonic signals considering that the underlying system is subject to multiplicative noises, additive noises and outliers. Furthermore, an outlier-resistant event-triggered mechanism is designed to prevent the transmission of unnecessary measurements and outliers. In order to guarantee the satisfactory filtering performance, this paper aims to design a recursive strong tracking filtering algorithm under the event-triggered mechanism, where an upper bound on the filtering error covariance matrix is obtained by solving a set of Riccati difference equations, and minimized to recursively compute the filter gain matrix. Finally, the effectiveness of the proposed algorithm is verified through carrying out two sets of simulations.

Keywords: power harmonic detection; outliers-resistant event-triggered mechanism; recursive strong tracking filtering algorithm; measurement outliers; communication resource constraints

1. Introduction

The past few years have witnessed the ever-growing development of distributed generation technologies in power systems (e.g., wind power, photovoltaics, and energy storage) [1−3]. For rectification/inversion, a large number of power electronic devices have been employed to solve the problem of power output instability. Nevertheless, it is noted that these nonlinear devices might cause serious power harmonic pollution, thereby leading to voltage/current distortion and even operation instability of power systems [4−6]. Given these implications, power harmonic detection is an effective way to ensure efficient energy utilization and power supply. Consequently, there remains a pressing need to tackle the harmonic detection issue in intricate environments.

Over the past decades, various harmonic detection methods have been developed to address the power harmonic pollution problem, e.g., the Fourier transform [7, 8], time-frequency domain analysis [9, 10], and Kalman filtering (KF) [11−13]. Among these technologies, the KF algorithm has attracted extensive research interest in recent years due to its simple structure and noise robustness [14], but has not performed well for transient harmonic detection. To address this issue, a maximum likelihood-based adaptive extended KF method has been presented in [15] by optimizing the process and measurement error covariance matrices to improve the detection accuracy of transient harmonics. It is worth noting that the strong tracking filtering is robust against system uncertainties and sudden state changes, and such a technology has been widely applied to deal with the problem of power quality disturbance detection [16−18]. Nevertheless, to the best of our knowledge, the problem of harmonic detection in complex environments has not yet gained adequate attention.

In order to monitor the dynamics of power signals accurately, phase measurement units with high sampling rates are installed at certain critical nodes in power systems (such as generating stations, substations, and distribution

stations [19]). In this case, it is inevitable that a large amount of measurements are generated. Due to the the limited communication bandwidth [20, 21], massive measurement transmissions might cause a great waste of resources and network-induced phenomena (e.g., the network congestion, time delay, and data dropout) [22−26], thereby seriously affecting the monitoring/filtering performance of the system. Along this direction, various effective information scheduling strategies have been developed including data compression methods, ethernet communication protocols, and event-triggered mechanisms.

It is worth noting that the event-triggered mechanism has received much research interest due to its simplicity and flexibility [27−29]. Different from the time-based periodic transmission strategy, the event-triggered mechanism determines when the measurements are to be transmitted by a dedicatedly designed triggering function. Various dynamic event-triggered mechanisms have been developed to further enhance the data transmission efficiency [30−32]. Nevertheless, due to sensor failures and severe external electromagnetic interferences, measurement outliers with large amplitudes might occur randomly in complex environments, which may incur wrong event-triggered execution and seriously affect the harmonic detection performance.

In recent years, there has been extensive research on dealing with measurement outliers, and the proposed strategies can be roughly categorized into two groups: 1) the passive robustness-based scheme; and 2) the active detection-based scheme [33−35]. For the former, the innovation term is constrained by setting a proper threshold parameter and a filter is designed to reduce the sensitivity of the filtering performance to outliers. Nevertheless, this method could not completely eliminate outlier effects on the filtering performance, and the transmitted outlier signal may occupy the limited communication bandwidth. For the latter, most existing detection methods are not applicable to the case of continuous outliers, and the design of the detection function may be challenging. With this in mind, a seemingly interesting research topic is to develop a novel scheme to accurately eliminate the outlier effects and correctly execute event generators.

Based on the above analysis, it is clear that the communication bandwidth constrains the transmission of power signals and measurement outliers, and this leads to excessive measurement bias that seriously deteriorates the power harmonic detection performance. To this end, this paper is devoted to investigating the problem of power harmonic detection with limited communication bandwidth and outliers. *The main contributions are highlighted from threefold: 1) a dynamic tracking model is established that takes into account both additive and multiplicative noises to accurately reflect the engineering reality of power harmonic detection; 2) an outlier-resistant event-triggered mechanism (ORETM) is designed to prevent the transmission of unnecessary measurements and outliers, thereby eliminating the effects of outliers and relieving the communication channel burden; and 3) a recursive strong tracking filtering algorithm is developed to realize the online detection of power harmonics.*

The rest of the paper is organized as follows. Section 2 establishes a dynamic tracking model for power harmonic detection and designs the ORETM to prevent the transmission of the unnecessary measurements and outliers. Section 3 gives the main objectives of this paper and shows the design process of the recursive filter. Section 4 verifies the effectiveness of the proposed algorithm through numerical simulations. Finally, some concluding comments are given in Section 5.

Notations: $\mathbb{N}$ denotes the set of natural numbers. $\mathrm{diag}\{*\}$ is a block-diagonal matrix. I represents the identity matrix of compatible dimension. M^T, M^{-1} and $\mathrm{tr}\{M\}$ stand for the transpose, inverse and trace of a square matrix M, respectively. $\mathrm{E}\{x\}$ is the expectation of the stochastic variable x. $\mathrm{row}_m\{*\}$ denotes $\mathrm{row}\{\underbrace{*,*,\cdots,*}_{m}\}$

2. Problem Formulation

2.1. Dynamic Tracking Model

A distorted voltage signal generally consists of multiple sinusoidal signals superimposed on each other, and the expression is as follows:

$$y(t)=\sum_{i=1}^{n}A_i(t)\sin(i\omega_0 t+\varphi_i(t)) \tag{1}$$

where $A_i(t)$ and $\varphi_i(t)$ represent, respectively, the amplitude and phase of the i-th ($i\in\{1,2,\cdots,n\}$) harmonic component and ω_0 is the fundamental angular frequency.

Define the state variable as follows [12]:

$$x(t)=\begin{bmatrix}x_1(t) & \dot{x}_1(t) & \cdots & x_n(t) & \dot{x}_n(t)\end{bmatrix}^T \tag{2}$$

where

$$x_i(t) \triangleq A_i(t)\sin(i\omega_0 t + \varphi_i(t)),$$
$$\dot{x}_i(t) \triangleq A_i(t) i\omega_0 \cos(i\omega_0 t + \varphi_i(t)).$$

The continuous-time state space expression for power harmonics is as follows:

$$\dot{x}(t) = \Phi x(t) + Bw(t) \tag{3}$$

where the state transition matrix Φ, the input matrix B, and the Gaussian white noise are, respectively, denoted as

$$\Phi = \mathrm{diag}\{\bar{\Phi}_1, \bar{\Phi}_2, \cdots, \bar{\Phi}_n\},$$
$$B = \mathrm{diag}\{\bar{B}_1, \bar{B}_2, \cdots, \bar{B}_n\},$$
$$w(t) = \mathrm{diag}\{\bar{w}_1(t), \bar{w}_2(t), \cdots, \bar{w}_n(t)\}.$$

Here, $\bar{\Phi}_i = \begin{bmatrix} 0 & 1 \\ -i\omega_0{}^2 & 0 \end{bmatrix}$, $\bar{B}_i = \begin{bmatrix} 0 \\ 1 \end{bmatrix}$, and $\bar{w}_i(t)$ follows the Gaussian distribution with zero mean and variance $\chi_i^2 \triangleq A_i^2/2\pi$.

It should be noted that in real power systems, power signals are usually subject to multiplicative and additive noises, mainly due to the phase mismatch and quantisation effects in the phasor measurement units. Taking into account the additive and multiplicative noises as well as measurement outliers, the discrete-time dynamic tracking model is established as follows:

$$x_{k+1} = (F + F_s\alpha_k)x_k + \bar{w}_k, \tag{4}$$

$$y_k = (C + C_s\beta_k)x_k + v_k + m_k \tag{5}$$

where

$$F = \mathrm{diag}\{\bar{F}_1, \bar{F}_2, \cdots, \bar{F}_n\},$$
$$\bar{w}_k = \mathrm{diag}\{\bar{w}_{1,k}, \bar{w}_{2,k}, \cdots, \bar{w}_{n,k}\}$$

with

$$\bar{F}_i = \begin{bmatrix} \cos(i\omega_0 T) & \dfrac{\cos(i\omega_0 T)}{i\omega_0} \\ -i\omega_0 \sin(i\omega_0 T) & \cos(i\omega_0 T) \end{bmatrix},$$
$$\bar{w}_{i,k} = \int_0^T \begin{bmatrix} \dfrac{\sin(\omega_0 T)}{\omega_0} \\ \cos(\omega_0 T) \end{bmatrix} \bar{w}_i(s)ds.$$

$C = \begin{bmatrix} 1 & 0 & 1 & 0 & \cdots & 1 & 0 \end{bmatrix}$ is the observation matrix; α_k and β_k are the multiplicative noises; F_s and C_s are the known real-valued matrices with dimensions consistent with the matrices F and C, respectively; v_k denotes the measurement noise; and m_k represents the measurement outliers.

In this paper, the noise statistics is shown as follows:

$$\mathrm{E}\{w_k\} = \mathrm{E}\{v_k\} = \mathrm{E}\{\alpha_k\} = \mathrm{E}\{\beta_k\} = 0,$$
$$\mathrm{E}\{\alpha_k w_l^T\} = \mathrm{E}\{\alpha_k v_l^T\} = \mathrm{E}\{\beta_k w_l^T\} = \mathrm{E}\{\beta_k v_l^T\} = 0,$$
$$\mathrm{E}\{\alpha_k \alpha_l^T\} = \delta_{kl}, \qquad \mathrm{E}\{\beta_k \beta_l^T\} = \delta_{kl},$$
$$\mathrm{E}\{w_k w_l^T\} = Q_k\delta_{kl}, \quad \mathrm{E}\{v_k v_l^T\} = R_k\delta_{kl},$$

where δ_{kl} is the Kronecker function; R_k is the measurement noise covariance matrix; and

$$Q_k = \mathrm{diag}\{\kappa\bar{Q}_{1,k}, \kappa\bar{Q}_{2,k}, \cdots, \kappa\bar{Q}_{n,k}\}$$

is the process noise covariance matrix with κ being an adjustable parameter and

$$\bar{Q}_{i,k} = \chi_i^2 \begin{bmatrix} \dfrac{2i\omega_0 T - \sin(2i\omega_0 T)}{4i^3\omega_0^3} & \dfrac{\sin^2(i\omega_0 T)}{2i^2\omega_0^2} \\ \dfrac{\sin^2(i\omega_0 T)}{2i^2\omega_0^2} & \dfrac{T}{2} + \dfrac{\sin(i\omega_0 T)}{4i\omega_0} \end{bmatrix}.$$

Remark 1: In real-world settings, the correlation between power harmonic signals is not negligible given the underlying system dynamics characteristics. In general, the covariance matrix of the process noise is predetermined as a unit matrix in conventional tracking models (e.g., the phase angle vector model and the orthogonal vector model), in which the correlation between state variables cannot be characterized. In contrast, the developed dynamic tracking model theoretically derives the process noise covariance matrix factoring in the correlation between state variables, and thus further enhancing the detection accuracy of power harmonics.

2.2. Outliers-Resistant Event-Triggered Mechanism

For the purpose of reducing the pressure on the communication channel and eliminating the effect of outliers on the filtering performance, an improved event-triggered mechanism is designed to determine when the measurement should be transmitted from the sensor to the remote filter. The event release instant sequence is denoted by $k_0 < k_1 < \cdots < k_t \cdots$ and satisfies

$$k_{t+1} = \inf_{k\in\mathbb{N}}\{k > k_t : \wp_1 + \eta\hbar_k < \left\|y_{k_t} - y_k\right\|^2 < \wp_2\} \tag{6}$$

where $\wp_1$ and $\wp_2$ are given positive scalar parameters; y_{k_t} and y_k denote the latest transmission value and the current measurement, respectively; and $\hbar_k$ is an auxiliary offset dynamic variable, which can be recursively calculated by

$$\hbar_{k+1} = \rho\hbar_k + \wp_1 - \left\|y_{k_t} - y_k\right\|^2, \quad \hbar_0 \geqslant 0. \tag{7}$$

Here, ρ and η are given positive scalar parameters satisfying $\rho \in (0,1)$ and $\eta \leqslant \rho$.

From (7), it follows that the current measurement y_k certainly satisfies one of the following three cases:

$$\begin{cases} y_k \in \aleph_{1,k} \triangleq \{y_k : \left\|y_{k_t} - y_k\right\|^2 \leqslant \wp_1 + \eta\hbar_k\} \\ y_k \in \aleph_{2,k} \triangleq \{y_k : \left\|y_{k_t} - y_k\right\|^2 \geqslant \wp_2\} \\ y_k \in \aleph_{3,k} \triangleq \{y_k : \wp_1 + \eta\hbar_k < \left\|y_{k_t} - y_k\right\|^2 < \wp_2\} \end{cases}. \tag{8}$$

It is worth clarifying that the obtained data packet y_k is an unnecessary measurement signal if $y_k \in \aleph_{1,k}$ and the data packet y_k is an outlier when $y_k \in \aleph_{2,k}$. The event generator is executed only if the data packet y_k satisfies $y_k \in \aleph_{3,k}$. Otherwise, the zero-order-hold scheme is adopted to update the signal $\tilde{y}_k$ accepted by the remote filter.

$$\tilde{y}_k = y_{k_t},\ k \in \{k_t, k_t + 1, \cdots k_{t+1} - 1\}. \tag{9}$$

Remark 2: The traditional saturation function-based outlier-resistant methods are capable of minimizing the effect of outliers on the filtering performance to some extent. Nevertheless, it is inevitable that measurement outliers are transmitted to the remote filter over the channel with limited bandwidth, which would impose additional communication burdens. As such, the event triggering function is redesigned in this paper to prevent the transmission of unnecessary measurements and outliers on the basis of the existing event-triggered mechanism [34]. Furthermore, the designed method avoids the need to design complex detection functions and is suitable to deal with outliers appearing continuously.

3. Filter Design Based on Outliers-resistant Event-triggered Mechanism

In this section, we are devoted to designing a recursive strong tracking filtering algorithm under the event-triggered mechanism, in which an upper bound on the filtering error covariance is guaranteed and minimized to derive the filtering gain matrix. Then, the strong tracking filtering idea is introduced to adjust the one-step prediction error covariance.

3.1. Filter Structure

Based on the state space model (4) and the measurement model (5), the structure of the proposed filter is established as

$$\hat{x}_{k+1|k} = F\hat{x}_{k|k}, \tag{10}$$

$$\hat{x}_{k+1|k+1} = \hat{x}_{k+1|k} + L_{k+1}(\tilde{y}_{k+1} - C\hat{x}_{k+1|k}) \tag{11}$$

where $\hat{x}_{k+1|k}$ and $\hat{x}_{k+1|k+1}$ denote, respectively, the one-step prediction and estimation of the state x_{k+1} at time $k+1$, and K_{k+1} is the filter gain matrix to be designed.

According to (10)–(11), the one-step prediction error $\tilde{x}_{k+1|k} \triangleq x_{k+1} - \hat{x}_{k+1|k}$ and the filtering error $\tilde{x}_{k+1|k+1} \triangleq x_{k+1} - \hat{x}_{k+1|k+1}$ are represented as

$$\tilde{x}_{k+1|k} = F\tilde{x}_{k|k} + F_s\alpha_k x_k + \omega_k, \tag{12}$$

$$\begin{aligned}\tilde{x}_{k+1|k+1} = {} & (I - L_{k+1}C)\tilde{x}_{k+1|k} - L_{k+1}C_s\beta_{k+1}x_{k+1} \\ & - L_{k+1}\sigma_{k+1} - L_{k+1}v_{k+1}\end{aligned} \tag{13}$$

where $\sigma_{k+1} \triangleq \tilde{y}_{k+1} - y_{k+1}$ denotes the non-triggering error. For ease of representation, we next give the following assumption about σ_{k+1}.

Assumption 1: The non-triggering error σ_{k+1} is approximated by the one at time k if $y_{k+1} \in \aleph_{2,k+1}$, i.e., $\sigma_{k+1} = \sigma_k$.

3.2. Filter Design

Before presenting the main results, we first introduce the following lemmas which will be of great help to the following filter design.

Lemma 1: [36] Suppose $\mathcal{X} = \mathcal{X}^T \leqslant 0$, $\mathcal{Y} = \mathcal{Y}^T \leqslant 0$, and define a matrix function $\Psi(\cdot): \mathbb{R}^{n\times n} \to \mathbb{R}^{n\times n}$. If $\forall \mathcal{X} \leqslant \mathcal{Y}$, $\Psi(\mathcal{X}) \leqslant \Psi(\mathcal{Y})$ holds, the solutions of the equations $\mathcal{M}_{k+1} \leqslant \Psi(\mathcal{M}_k)$ and $\mathcal{N}_{k+1} = \Psi(\mathcal{N}_k)$ satisfy $\mathcal{M}_k \leqslant \mathcal{N}_k$.

Lemma 2: [37] For arbitrary matrices $\mathcal{A}$ and $\mathcal{B}$ of appropriate dimensions, there is positive scalar λ such that the following inequality holds:

$$\mathcal{A}\mathcal{B}^T + \mathcal{B}\mathcal{A}^T \leq \lambda\mathcal{A}\mathcal{A}^T + \lambda^{-1}\mathcal{B}\mathcal{B}^T. \tag{14}$$

Lemma 3: [38] The upper bound on the non-triggering error satisfies the following inequality relationship:

$$\sigma_k^T\sigma_k \leqslant (\eta^2 + \eta)\bar{X}_k^2 + (1+\eta)\wp_1^2 \tag{15}$$

where

$$\begin{aligned}\bar{X}_{k+1} = {} & \left[(1+\lambda_1)(1+\lambda_2)\rho^2 + \left(1+\lambda_1^{-1}\right)\left(\eta^2+\eta\right)\right]\bar{X}_k \\ & + \left[(1+\lambda_1)\left(1+\lambda_2^{-1}\right) + \left(1+\lambda_1^{-1}\right)(1+\eta)\right]\wp_1^2\end{aligned}$$

with λ_1 and λ_2 being known scalars.

Proof: This lemma can be easily proved by referring to [38], and the proof is thus omitted for conciseness.

Lemma 4: [13] The state covariance $\bar{X}_{k+1} \triangleq \mathrm{E}\{x_{k+1}x_{k+1}^T\}$ is represented as

$$\bar{X}_{k+1|k+1} = F\bar{X}_{k|k}F^T + F_s\bar{X}_{k|k}F_s^T + Q_k \tag{16}$$

with the initial state covariance $\bar{X}_{0|0} = \hat{x}_{0|0} + P_{0|0}$.

Proof: Based on the discrete state space expression (4), we have

$$\begin{aligned}\bar{X}_{k+1} = {} & F\mathrm{E}\{x_k x_k^T\}F^T + F_s\mathrm{E}\{\alpha_k x_k x_k^T \alpha_k^T\}F_s^T \\ & + \mathrm{E}\{\omega_k\omega_k^T\} + F_{1,k} + F_{1,k}^T \\ & + F_{2,k} + F_{2,k}^T + F_{3,k} + F_{3,k}^T\end{aligned} \tag{17}$$

where

$$\begin{aligned}F_{1,k} &\triangleq F\mathrm{E}\{x_k x_k^T \alpha_k^T\}F_s^T, \\ F_{2,k} &\triangleq F_s\mathrm{E}\{\alpha_k x_k \omega_k^T\}, \\ F_{3,k} &\triangleq F\mathrm{E}\{x_k\omega_k^T\}.\end{aligned}$$

Obviously, we can obtain that $F_{1,k}$, $F_{2,k}$, and $F_{3,k}$ are zeros. Thus, it is easy to conclude that (16) holds.

Theorem 1: Consider the ORETM (6) and the filter (10)-(11). There exist positive scalars ξ_1 and ξ_2 such that the upper bound $\Sigma_{k+1|k}$ on the one-step prediction error covariance $P_{k+1|k} \triangleq \mathrm{E}\{\tilde{x}_{k+1|k}\tilde{x}_{k+1|k}^T\}$ and the upper bound $\Sigma_{k+1|k+1}$ on the filtering error covariance $P_{k+1|k+1} \triangleq \mathrm{E}\{\tilde{x}_{k+1|k+1}\tilde{x}_{k+1|k+1}^T\}$ are derived in the following form:

$$\Sigma_{k+1|k} = F\Sigma_{k|k}F^T + F_s\bar{X}_k F_s^T + Q_k, \tag{18}$$

$$\begin{aligned}\Sigma_{k+1|k+1} = {} & (1+\xi_1)(I - L_{k+1}C)\Sigma_{k+1|k} \\ & \times (I - L_{k+1}C)^T + L_{k+1}C_s\bar{X}_{k+1}C_s^T L_{k+1}^T \\ & + (1+\xi_1{}^{-1} + \xi_2)L_{k+1}(\Theta_{k+1}I)L_{k+1}^T \\ & + (1+\xi_2^{-1})L_{k+1}R_{k+1}L_{k+1}^T\end{aligned} \tag{19}$$

where

$$\Theta_{k+1} \triangleq (\eta^2+\eta)\bar{X}_k^2 + (1+\eta)\wp_1^2.$$

Then the matrix $\Sigma_{k+1|k+1}$ can be minimized by designing the filter gain matrix as

$$L_{k+1} = \Pi_{k+1}\Xi_{k+1}^{-1} \tag{20}$$

where

$$\begin{aligned}\Pi_{k+1} &\triangleq (1+\xi_1)\Sigma_{k+1|k}C^T,\\ \Xi_{k+1} &\triangleq (1+\xi_1)C\Sigma_{k+1|k}C^T + C_s\bar{X}_{k+1}C_s^T\\ &\quad + (1+\xi_1{}^{-1}+\xi_2)(\Theta_{k+1}I) + (1+\xi_2^{-1})R_{k+1}.\end{aligned}$$

Proof: From (12), the one-step prediction error covariance is written as

$$\begin{aligned}P_{k+1|k} &= F\mathrm{E}\{\tilde{x}_{k|k}\tilde{x}_{k|k}^T\}F^T + F_s\mathrm{E}\{\alpha_k x_k x_k^T \alpha_k^T\}F_s^T\\ &\quad + \mathrm{E}\{\omega_k\omega_k^T\} + F_{1,k} + F_{1,k}^T\\ &\quad + F_{2,k} + F_{2,k}^T + F_{3,k} + F_{3k}^T\end{aligned} \tag{21}$$

where

$$\begin{aligned}F_{1,k} &\triangleq F\mathrm{E}\{\tilde{x}_{k|k}x_k^T\alpha_k^T\}F_s^T,\\ F_{2,k} &\triangleq F_s\mathrm{E}\{\alpha_k x_k w_k^T\},\\ F_{3,k} &\triangleq F\mathrm{E}\{\tilde{x}_{k|k}\omega_k^T\}.\end{aligned}$$

It is obvious that $F_{1,k}$, $F_{2,k}$, and $F_{3,k}$ are zeros. Hence, the one-step prediction error covariance is updated as

$$P_{k+1|k} = FP_{k|k}F^T + F_s\bar{X}_kF_s^T + Q_k. \tag{22}$$

In addition, the filtering error covariance $P_{k+1|k+1}$ can be obtained from (13) as

$$\begin{aligned}P_{k+1|k+1} &= (I-L_{k+1}C)\mathrm{E}\{\tilde{x}_{k+1|k}\tilde{x}_{k+1|k}^T\}(I-L_{k+1}C)^T\\ &\quad + L_{k+1}C_s\mathrm{E}\{\beta_{k+1}x_{k+1}x_{k+1}^T\beta_{k+1}^T\}C_s^TL_{k+1}^T\\ &\quad + L_{k+1}\mathrm{E}\{\sigma_{k+1}\sigma_{k+1}^T\}L_{k+1}^T\\ &\quad + L_{k+1}\mathrm{E}\{v_{k+1}v_{k+1}^T\}L_{k+1}^T - \aleph_{1,k+1} - \aleph_{1,k+1}^T\\ &\quad - \aleph_{2,k+1} - \aleph_{2,k+1}^T - \aleph_{3,k+1} - \aleph_{3,k+1}^T + \aleph_{4,k+1}\\ &\quad + \aleph_{4,k+1}^T + \aleph_{5,k+1} + \aleph_{5,k+1}^T + \aleph_{6,k+1} + \aleph_{6,k+1}^T\end{aligned} \tag{23}$$

where

$$\begin{aligned}\aleph_{1,k+1} &\triangleq (I-L_{k+1}C)\mathrm{E}\{\tilde{x}_{k+1|k}x_{k+1}^T\beta_{k+1}^T\}C_s^TL_{k+1}^T,\\ \aleph_{2,k+1} &\triangleq (I-L_{k+1}C)\mathrm{E}\{\tilde{x}_{k+1|k}\sigma_{k+1}^T\}L_{k+1}^T,\\ \aleph_{3,k+1} &\triangleq (I-L_{k+1}C)\mathrm{E}\{\tilde{x}_{k+1|k}v_{k+1}\}L_{k+1}^T,\\ \aleph_{4,k+1} &\triangleq L_{k+1}C_s\mathrm{E}\{\beta_{k+1}x_{k+1}\sigma_{k+1}^T\}L_{k+1}^T,\\ \aleph_{5,k+1} &\triangleq L_{k+1}C_s\mathrm{E}\{x_{k+1}\beta_{k+1}v_{k+1}^TL_{k+1}^T\},\\ \aleph_{6,k+1} &\triangleq L_{k+1}\mathrm{E}\{\sigma_{k+1}v_{k+1}^T\}L_{k+1}^T.\end{aligned}$$

Similarly, $\aleph_{1,k}$, $\aleph_{3,k}$, $\aleph_{4,k}$, and $\aleph_{5,k}$ are zeros. Applying Lemma 2 to the uncertainty terms $\aleph_{2,k+1}$ and $\aleph_{6,k+1}$, the following inequality relationships hold:

$$\begin{aligned}&-\aleph_{2,k+1} - \aleph_{2,k+1}^T\\ &\leqslant \xi_1(I-L_{k+1}C)\mathrm{E}\{\tilde{x}_{k+1|k}\tilde{x}_{k+1|k}^T\}(I-L_{k+1}C)^T\\ &\quad + \xi_1^{-1}L_{k+1}\mathrm{E}\{\sigma_{k+1}\sigma_{k+1}^T\}L_{k+1}^T,\end{aligned} \tag{24}$$

$$\begin{aligned}&\aleph_{6,k+1} + \aleph_{6,k+1}^T\\ &\leqslant \xi_2L_{k+1}\mathrm{E}\{\sigma_{k+1}\sigma_{k+1}^T\}L_{k+1}^T\\ &\quad + \xi_2^{-1}L_{k+1}\mathrm{E}\{v_{k+1}v_{k+1}^T\}L_{k+1}^T.\end{aligned} \tag{25}$$

It follows from Lemma 3 that

$$\mathrm{E}\{\sigma_{k+1}\sigma_{k+1}^T\}\leqslant\mathrm{E}\{\sigma_{k+1}^T\sigma_{k+1}\}I=\Theta_{k+1}I. \tag{26}$$

Substituting (24)-(26) into (23), we have

$$\begin{aligned}P_{k+1|k+1}\leqslant&(1+\xi_1)(I-L_{k+1}C)P_{k+1|k}\\&\times(I-L_{k+1}C)^T+L_{k+1}C_s\bar{X}_{k+1}C_s^TL_{k+1}^T\\&+(1+\xi_1^{-1}+\xi_2)L_{k+1}(\Theta_{k+1}I)L_{k+1}^T\\&+(1+\xi_2^{-1})L_{k+1}R_{k+1}L_{k+1}^T.\end{aligned} \tag{27}$$

It is obvious from (19) and (27) that $\Sigma_{k+1|k+1}=\Psi(\Sigma_{k|k})$ and $P_{k+1|k+1}\leqslant\Psi(P_{k|k})$. It follows from Lemma 1 that $\Sigma_{k+1|k}$ and $\Sigma_{k+1|k+1}$ are, respectively, the upper bounds of the one-step prediction error covariance $P_{k+1|k}$ and the filtering error covariance $P_{k+1|k+1}$, i.e., $P_{k+1|k}\leqslant\Sigma_{k+1|k}$ and $P_{k+1|k+1}\leqslant\Sigma_{k+1|k+1}$.

Subsequently, the filter gain matrix L_{k+1} is obtained by minimizing the matrix $\Sigma_{k+1|k+1}$. In accordance with (19), the matrix $\Sigma_{k+1|k+1}$ can be reorganized as

$$\begin{aligned}\Sigma_{k+1|k+1}=&(1+\xi_1)\Sigma_{k+1|k}-(1+\xi_1)(\Sigma_{k+1|k}C^TL_{k+1}^T\\&\times L_{k+1}C\Sigma_{k+1|k})+(1+\xi_1)L_{k+1}C\Sigma_{k+1|k}C^TL_{k+1}^T\\&+L_{k+1}C_s\bar{X}_{k+1}C_s^TL_{k+1}^T+(1+\xi_1{}^{-1}+\xi_2)\\&\times L_{k+1}(\Theta_{k+1}I)L_{k+1}^T+(1+\xi_2^{-1})L_{k+1}R_{k+1}L_{k+1}^T\\=&L_{k+1}\Xi_{k+1}L_{k+1}^T-\Pi_{k+1}^TL_{k+1}^T\\&-L_{k+1}\Pi_{k+1}+(1+\xi_1)\Sigma_{k+1|k}\\=&(L_{k+1}-\Pi_{k+1}\Xi_{k+1}^{-1})\Xi_{K+1}(L_{k+1}-\Pi_{k+1}\Xi_{k+1}^{-1})^T\\&-\Pi_{k+1}\Xi_{k+1}^{-1}\Pi_{k+1}^T+(1+\xi_1)\Sigma_{k+1|k}.\end{aligned} \tag{28}$$

It can be seen from (28) that the upper bound $\Sigma_{k+1|k+1}$ on the filtering error covariance can be minimized by designing $L_{k+1}=\Pi_{k+1}\Xi_{k+1}^{-1}$. The proof is now complete.

In order to ensure the filtering accuracy and outlier robustness, the strong tracking filtering is introduced to optimize the designed recursive algorithm [17]. Specifically, the prediction error covariance matrix $P_{k+1|k}$ is adjusted according to residuals. By introducing a scaling factor λ_{k+1}, the prediction error covariance $P_{k+1|k}$ from (22) is reformulated as

$$P_{k+1|k}=\lambda_{k+1}FP_{k|k}F^T+F_s\bar{X}_kF_s^T+Q_k, \tag{29}$$

and the scaling factor λ_{k+1} is calculated by

$$\lambda_k=\begin{cases}\bar{\lambda}_{k+1}, & \bar{\lambda}_{k+1}\geqslant1\\1, & \text{otherwise}\end{cases} \tag{30}$$

where

$$\begin{aligned}\bar{\lambda}_{k+1}&\triangleq\frac{\mathrm{tr}\{N_{k+1}\}}{\mathrm{tr}\{M_{k+1}\}},\\N_{k+1}&\triangleq V_{k+1}-\vartheta R_{k+1},\\M_{k+1}&\triangleq CFP_{k|k}F^TC^T,\end{aligned}$$

and V_{k+1} denotes the covariance matrix of the actual output residual, which can be obtained by

$$V_{k+1}=\begin{cases}\varepsilon_1\varepsilon_1^T, & k=1\\\dfrac{\varrho V_k+\varepsilon_{k+1}\varepsilon_{k+1}^T}{1+\varrho}, & k\geqslant1\end{cases}. \tag{31}$$

Here, $\varepsilon_{k+1}\triangleq y_{k+1}-C\hat{x}_{k+1|k}$ is the residual at $k+1$, ϱ is the forgetting factor with $0<\varrho<1$, and $\vartheta>1$ is the weakening factor.

Remark 3: Until now, our research has focused on the problem of power harmonic detection in the presence of communication bandwidth constraints and measurement outliers. Our results differ from existing ones in three distinct aspects: 1) the power harmonic detection challenge is addressed, for the first time, in the presence of multiplicative noises and the event-triggered mechanism; 2) the multiplicative uncertainties and non-triggering errors are encapsulated within a minimized upper bound of the filtering error covariance; and 3) a tailored recursive strong

tracking filtering algorithm is designed for power harmonics which is available for online applications.

4. Simulation Results and Analysis

In order to verify the efficacy of the proposed filtering algorithm with limited communication bandwidth and measurement outliers, the following three different algorithms are used for performance comparison.

1) **Algorithm 1**: the designed ORETM is utilized and this is the proposed recursive strong tracking filtering algorithm.

2) **Algorithm 2**: the designed ORETM is utilized and this is a recursive filtering algorithm without introducing the idea of strong tracking filtering.

3) **Algorithm 3**: a traditional dynamic event-triggered mechanism is employed [38], in which outliers are able to be transmitted to the remote filter, and this is the standard KF algorithm without considering non-triggering errors.

As can be found, the comparison of Algorithms 1 and 2 aims to verify the effectiveness of the strong tracking filtering idea in improving the performance of the recursive filtering algorithm. By comparing Algorithm 2 and Algorithm 3, the efficacy of the designed recursive filtering algorithm will be verified, and the effect of the designed ORETM will be demonstrated in terms of conserving network resources and removing outliers.

In this paper, we set the multiplicative noise matrix F_s and C_s to be $F_{s,k} = 0.01I$ and $C_{s,k} = \text{row}_{2n}\{0.01\}$. The associated filter parameters are chosen as $\xi_1 = 0.001$, $\xi_2 = 0.1$, $\varrho = 0.95$ and $\vartheta = 2$. Moreover, the triggering parameters are set to be $\wp_1 = 2.4$, $\wp_2 = 12.9$, $\rho = 0.2$ and $\eta = 0.1$. In this paper, the commonly used trial-and-error method is adopted by appropriately selecting $\wp_1$, $\wp_2$, ρ and η.

4.1. Fundamental Voltage Signal with Amplitude Sags and Phase Jumps

The fundamental voltage signal is expressed as

$$y_k = (1 + 0.01\beta_k)A_{1,k}\sin(\omega kT + \varphi_{1,k}) + v_k + m_k$$

where

$$A_{1,k} = \begin{cases} 220\sqrt{2}, & 0 \leqslant k \leqslant 450 \\ 0.6 \times 220\sqrt{2}, & 450 \leqslant k \leqslant 750 \\ 220\sqrt{2}, & 750 \leqslant k \leqslant 1000 \end{cases},$$

$$\varphi_{1,k} = \begin{cases} \pi/4, & 0 \leqslant k \leqslant 450 \\ 0, & 450 \leqslant k \leqslant 750 \\ \pi/4, & 750 \leqslant k \leqslant 1000 \end{cases}.$$

Figure 1 illustrates a voltage signal with amplitude sags and phase jumps, where the outliers occur randomly. Figure 2 shows the DTRs with different triggering thresholds $\wp_1$ and $\wp_2$. It can be seen from Figure 2 that the DTR continuously reduces when the parameter $\wp_1$ increases and the parameter $\wp_2$ decreases, thus saving a large amount of communication resources. This is due to the fact that the designed ORETM is capable of preventing the transmission of unnecessary measurements and outliers by adjusting the two thresholds. Accordingly, it is of great significance to select appropriate triggering thresholds according to the actual engineering requirements.

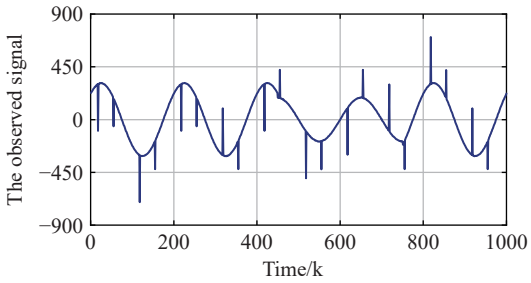

Figure 1. The fundamental voltage transient signal with outliers.

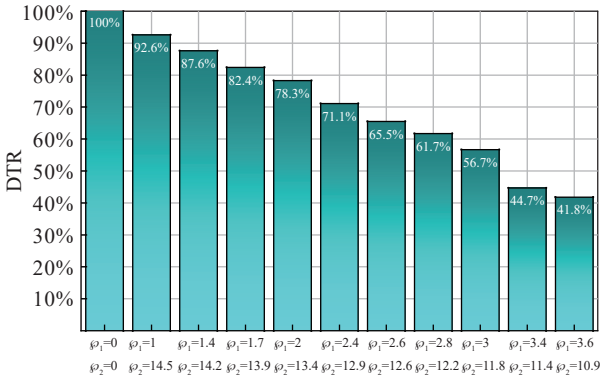

Figure 2. The DTRs with different triggering thresholds.

The effectiveness of the proposed algorithm is verified by the comparison with Algorithms 2 and 3 when the DTR is only 71.1% ($\varphi_1 = 2.4$ and $\varphi_2 = 12.9$). The detection results for the voltage amplitude and phase are shown in Figure 3–Figure 4. It is observed that Algorithm 3 has a large tracking error due to the effect of outliers. It can be found that the filtering accuracy of Algorithms 1 and 2 is higher than that of Algorithm 3 due to outlier elimination by the designed ORETM. Furthermore, the proposed recursive strong tracking filtering algorithm (i.e., Algorithm 3) outperforms Algorithm 2 in the case of sudden signal changes.

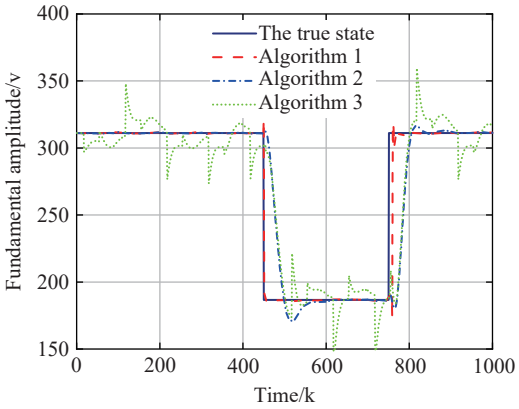

Figure 3. The true state and estimate of the fifth harmonic component.

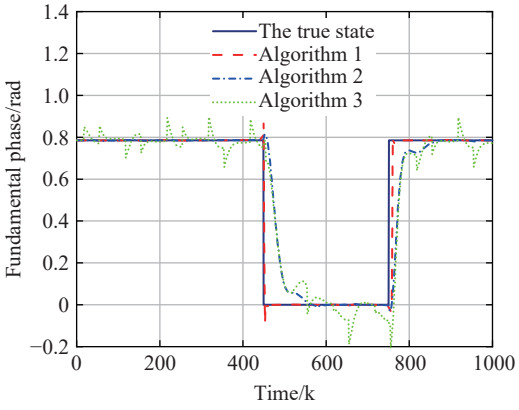

Figure 4. The true state and estimate of the fifth harmonic component.

4.2. Distorted Voltage Signal

The harmonic swell signal is expressed as

$$\begin{aligned} y_k = {} & (1+0.01\beta_k)A_1 \sin(\omega kT + \varphi_1) \\ & + (1+0.01\beta_k)A_{3,k} \sin(3\omega kT + \varphi_{3,k}) \\ & + (1+0.01\beta_k)A_{5,k} \sin(5\omega kT + \varphi_{5,k}) + v_k + m_k \end{aligned}$$

where

$$A_{1,k} = 220\sqrt{2}, \quad \varphi_{1,k} = 0$$

$$A_{3,k} = \begin{cases} 0.4\times 220\sqrt{2}, & 0 \leqslant k \leqslant 450 \\ 0.6\times 220\sqrt{2}, & 450 \leqslant k \leqslant 750 \\ 0.4\times 220\sqrt{2}, & 750 \leqslant k \leqslant 1000 \end{cases},$$

$$\varphi_{3,k} = \begin{cases} \pi/10, & 0 \leqslant k \leqslant 450 \\ \pi/3, & 450 \leqslant k \leqslant 750 \\ \pi/10, & 750 \leqslant k \leqslant 1000 \end{cases}$$

$$A_{5,k} = \begin{cases} 0.2\times 220\sqrt{2}, & 0 \leqslant k \leqslant 450 \\ 0.4\times 220\sqrt{2}, & 450 \leqslant k \leqslant 750 \\ 0.2\times 220\sqrt{2}, & 750 \leqslant k \leqslant 1000 \end{cases},$$

$$\varphi_{5,k} = \begin{cases} \pi/12, & 0 \leqslant k \leqslant 450 \\ \pi/4, & 450 \leqslant k \leqslant 750 \\ \pi/12, & 750 \leqslant k \leqslant 1000 \end{cases}$$

Figure 5 plots a voltage signal with the amplitude and phase swell, harmonic distortion, and outliers. The trend of DTR with different thresholds is shown in Figure 6. In addition, the effectiveness of the proposed algorithm is further verified by setting $\wp_1 = 2.4$ and $\wp_2 = 12.9$, at which the DTR is 72.4%. Figure 7–Figure 10 show the results of three filtering algorithms in detecting the voltage amplitude and phase of the third and fifth harmonic components. It is observed that the tracking delay is apparent as the order increases for detecting harmonic components of different orders. Nevertheless, the detection accuracy of the proposed algorithm is acceptable and its performance is optimal among the three algorithms. Summarizing the above discussions, it is verified that the developed recursive strong tracking filtering algorithm is capable of achieving accurate power harmonic detection in the presence of limited communication bandwidth and outliers under transient conditions.

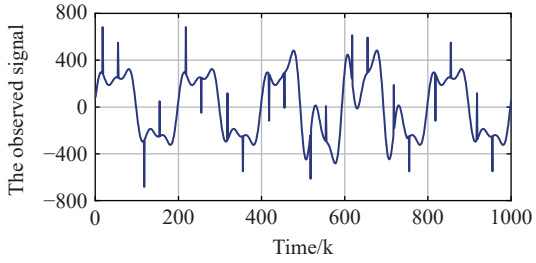

Figure 5. The harmonic transient signal with outliers.

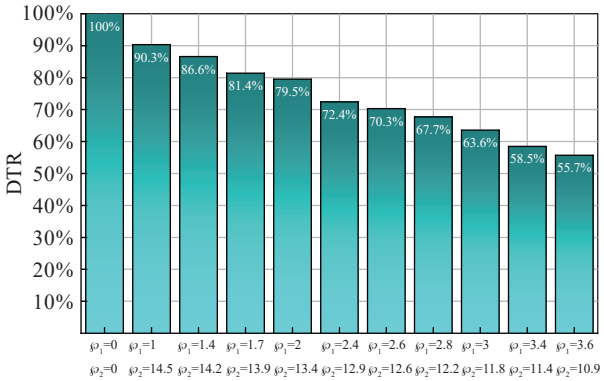

Figure 6. The DTRs with different triggering thresholds.

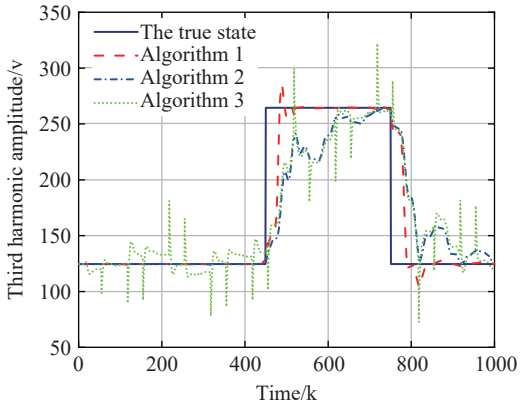

Figure 7. The third harmonic amplitude and its estimates with different algorithms.

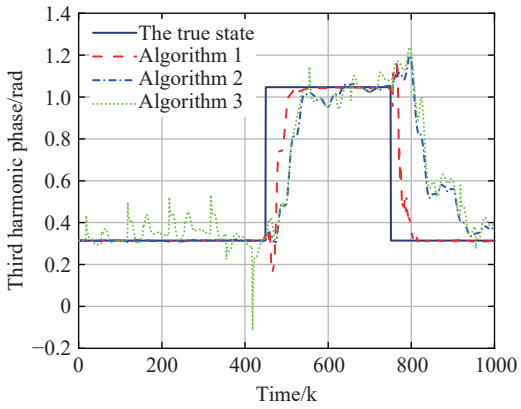

Figure 8. The third harmonic phase and its estimates with different algorithms.

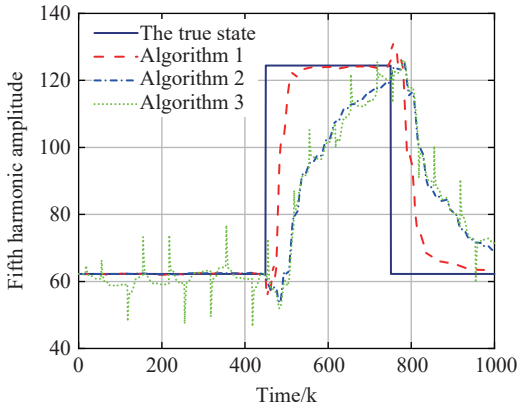

Figure 9. The fifth harmonic amplitude and its estimates with different algorithms.

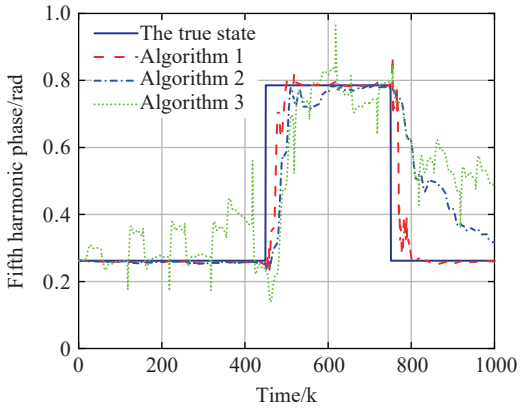

Figure 10. The fifth harmonic phase and its estimates with different algorithms.

5. Conclusion

In this paper, we have investigated the problem of transient harmonic detection in the presence of multiplicative noises, limited communication bandwidth, and measurement outliers. First, the dynamic behavior of the harmonic signals has been described by the established dynamic state-space model, where the process noise covariance matrix has been obtained computationally rather than a priori. Second, the ORETM has been designed to prevent the transmission of unnecessary measurements and outliers by appropriately setting the triggering parameters. Then, a recursive strong tracking filtering algorithm has been developed by taking into account the non-triggered error, in which an upper bound on the filtering error covariance has been derived and minimized to obtain the filtering gain matrix. Finally, the effectiveness of the proposed filtering algorithm has been verified by implementing two sets of numerical simulations. Future research topics include 1) power harmonic detection in the presence of non-Gaussian noises; and 2) multi-sensor network based distributed detection for power harmonics.

Author Contributions: Algorithm design was accomplished by **Xingzhen Bai**. Material preparation, model construction were performed by **Liqun Yu** and **Yufeng Sun**. The first draft of the manuscript was written by **Guhui Li** and **Mingyu Ding** and all authors commented on previous versions of the manuscript.

Funding: This work was supported in part by the National Natural Science Foundation of China under Grants 62273211.

Data Availability Statement: Not applicable.

Conflicts of Interest: The authors declare no conflict of interest.

Acknowledgments: We would like to thank the project team members of the National Natural Science Foundation of China who encouraged this research.

References

1. Chen, W.; Liu, L.; Liu, G.P. Privacy-preserving distributed economic dispatch of microgrids: A dynamic quantization-based consensus scheme with homomorphic encryption. IEEE Trans. Smart Grid, **2023**, *14*: 701−713. doi: 10.1109/TSG.2022.3189665
2. Fang, Z.; Lin, Y.Z.; Song, S.; *et al*. State estimation for situational awareness of active distribution system with photovoltaic power plants. IEEE Trans. Smart Grid, **2021**, *12*: 239−250. doi: 10.1109/TSG.2020.3009571
3. Qu, B.G.; Wang, Z.D.; Shen, B.; *et al*. Outlier-resistant recursive state estimation for renewable-electricity-generation-based microgrids. IEEE Trans. Ind. Inf., **2023**, *19*: 7133−7144. doi: 10.1109/TII.2022.3205354
4. Eroğlu, H.; Cuce, E.; Cuce, P.M.; *et al*. Harmonic problems in renewable and sustainable energy systems: A comprehensive review. Sustain. Energy Technol. Assessm., **2021**, *48*: 101566. doi: 10.1016/j.seta.2021.101566
5. Kettner, A.M.; Reyes-Chamorro, L.; Becker, J.K.M.; *et al*. Harmonic power- flow study of polyphase grids with converter-interfaced distributed energy resources–Part I: Modeling framework and algorithm. IEEE Trans. Smart Grid, **2022**, *13*: 458−469. doi: 10.1109/TSG.2021.3120108
6. Sun, Y.Y.; Xie, X.M.; Zhang, L.H.; *et al*. A voltage adaptive dynamic harmonic model of nonlinear home appliances. IEEE Trans. Ind. Electron., **2020**, *67*: 3607−3617. doi: 10.1109/TIE.2019.2921261
7. Deng, Y.; Zhao, G.J.; Zhu, K.H.; *et al*. NCAFI: Nuttall convolution window all-phase FFT interpolation-based harmonic detection algorithm for infrared imaging detection. Infrared Phys. Technol., **2022**, *125*: 104310. doi: 10.1016/j.infrared.2022.104310
8. Su, T.X.; Yang, M.F.; Jin, T.; *et al*. Power harmonic and interharmonic detection method in renewable power based on Nuttall double-window all-phase FFT algorithm. IET Renew. Power Generat., **2018**, *12*: 953−961. doi: 10.1049/iet-rpg.2017.0115
9. Kapisch, E.B.; Filho, L.M.A.; Silva, L.R.M.; *et al*. Novelty detection in power quality signals with surrogates: A time-frequency technique. In *Proceedings of 2020 International Conference on Systems, Signals and Image Processing, Niteroi, Brazil, 01-03 July 2020*; IEEE: New York, 2020; pp. 373–378. doi:10.1109/IWSSIP48289.2020.9145149
10. Wu, J.Z.; Mei, F.; Chen, C.; *et al*. Harmonic detection method in power system based on empirical wavelet transform. Power System Protection and Control, **2020**, *48*: 136−143. doi: 10.19783/j.cnki.pspc.190470
11. Bagheri, A.; Mardaneh, M.; Rajaei, A.; *et al*. Detection of grid voltage fundamental and harmonic components using Kalman filter and generalized averaging method. IEEE Trans. Power Electron., **2016**, *31*: 1064−1073. doi: 10.1109/TPEL.2015.2418271
12. Nie, X.H. Detection of grid voltage fundamental and harmonic components using Kalman filter based on dynamic tracking model. IEEE Trans. Ind. Electron., **2020**, *67*: 1191−1200. doi: 10.1109/TIE.2019.2898626
13. Qu, B.G.; Li, N.; Liu, Y.R.; *et al*. Estimation for power quality disturbances with multiplicative noises and correlated noises: A recursive estimation approach. Int. J. Syst. Sci., **2020**, *51*: 1200−1217. doi: 10.1080/00207721.2020.1755476
14. Nie, H.Y.; Nie, X.H. Research on dynamic modeling of KF algorithm for detecting distorted AC signal. Energies, **2021**, *14*: 8175. doi: 10.3390/en14238175
15. Xi, Y.H.; Li, Z.W.; Zeng, X.J.; *et al*. Detection of voltage sag using an adaptive extended Kalman filter based on maximum likelihood. J. Electr. Eng. Technol., **2017**, *12*: 1016−1026. doi: 10.5370/JEET.2017.12.3.1016
16. Chen, X.J.; Li, K.C.; Xiao, J. Classification of power quality disturbances using dual strong tracking filters and rule-based extreme learning machine. Int. Trans. Electr. Energy Syst., **2018**, *28*: e2560. doi: 10.1002/etep.2560
17. He, S.F.; Li, K.C.; Zhang, M. A new transient power quality disturbances detection using strong trace filter. IEEE Trans. Instrum.

Meas., **2014**, *63*: 2863−2871. doi: 10.1109/TIM.2014.2326762
18. Pramanik, M.; Routray, A.; Mitra, P. A two-stage adaptive symmetric-strong-tracking square-root cubature Kalman filter for harmonics and interharmonics estimation. Electr. Power Syst. Res., **2022**, *210*: 108133. doi: 10.1016/j.epsr.2022.108133
19. Seger, P.V.H.; Grando, F.L.; Lazzaretti, A.E.; *et al*. Power system monitoring through low-voltage distribution network using *freePMU*. *IEEE Trans. Ind. Applicat*. **2022**, *58*, 3153–3163. doi:10.1109/TIA.2022.3151045
20. Bai, X.Z.; Zheng, X.L.; Ge, L.J.; *et al*. Event-triggered forecasting-aided state estimation for active distribution system with distributed generations. Front. Energy Res., **2021**, *9*: 707183. doi: 10.3389/fenrg.2021.707183
21. Cheng, C.; Bai, X.Z. Robust forecasting-aided state estimation in power distribution systems with event-triggered transmission and reduced mixed measurements. IEEE Trans. Power Syst., **2021**, *36*: 4343−4354. doi: 10.1109/TPWRS.2021.3062386
22. Hu, J.; Wang, Z.D.; Liu, S.; *et al*. A variance-constrained approach to recursive state estimation for time-varying complex networks with missing measurements. Automatica, **2016**, *64*: 155−162. doi: 10.1016/j.automatica.2015.11.008
23. Li, Q.; Wang, Z.D.; Shen, B.; *et al*. A resilient approach to recursive distributed filtering for multirate systems over sensor networks with time-correlated fading channels. IEEE Trans. Signal Inf. Process. Over Networks, **2021**, *7*: 636−647. doi: 10.1109/TSIPN.2021.3117366
24. Qian, W.; Gao, Y.S.; Yang, Y. Global consensus of multiagent systems with internal delays and communication delays. IEEE Trans. Syst. Man Cybern. Syst., **2019**, *49*: 1961−1970. doi: 10.1109/TSMC.2018.2883108
25. Qian, W.; Xing, W.W.; Fei, S. M. H_∞ state estimation for neural networks with general activation function and mixed time-varying delays. IEEE Trans. Neural Netw. Learn. Syst., **2021**, *32*: 3909−3918. doi: 10.1109/TNNLS.2020.3016120
26. Zhao, Z.Y.; Wang, Z.D.; Zou, L.; *et al*. Set-membership filtering for time-varying complex networks with uniform quantisations over randomly delayed redundant channels. International Journal of Systems Science, **2020**, *51*: 3364−3377. doi: 10.1080/00207721.2020.1814898
27. Bai, X.Z.; Wang, Z.D.; Zou, L.; *et al*. Target tracking for wireless localization systems using set-membership filtering: A component-based event-triggered mechanism. Automatica, **2021**, *132*: 109795. doi: 10.1016/j.automatica.2021.109795
28. Rahimi, F.; Rezaei, H. An event-triggered recursive state estimation approach for time-varying nonlinear complex networks with quantization effects. Neurocomputing, **2021**, *426*: 104−113. doi: 10.1016/j.neucom.2020.09.074
29. Yu, Y.J.; Dong, H.L.; Wang, Z.D.; *et al*. Delay-distribution-dependent non-fragile state estimation for discrete-time neural networks under event-triggered mechanism. Neural Comput. Applicat., **2019**, *31*: 7245−7256. doi: 10.1007/s00521-018-3516-z
30. Ge, X.H.; Han, Q.L.; Wang, Z.D. A dynamic event-triggered transmission scheme for distributed set-membership estimation over wireless sensor networks. IEEE Trans. Cybern., **2019**, *49*: 171−183. doi: 10.1109/TCYB.2017.2769722
31. Wang, S.Y.; Wang, Z.D.; Dong, H.L.; *et al*. A dynamic event-triggered approach to recursive nonfragile filtering for complex networks with sensor saturations and switching topologies. IEEE Trans. Cybern., **2022**, *52*: 11041−11054. doi: 10.1109/TCYB.2021.3049461
32. Yi, X.L.; Liu, K.; Dimarogonas, D.V.; *et al*. Dynamic event-triggered and self-triggered control for multi-agent systems. IEEE Trans. Automat. Control, **2019**, *64*: 3300−3307. doi: 10.1109/TAC.2018.2874703
33. Fang, H.Z.; Haile, M.A.; Wang, Y.B. Robustifying the Kalman filter against measurement outliers: An innovation saturation mechanism. In *Proceedings of 2018 IEEE Conference on Decision and Control, Miami, FL, USA, 17-19 December 2018*; IEEE: New York, 2018; pp. 6390–6395. doi:10.1109/CDC.2018.8619140
34. Zhao, X.; Liu, C.S.; Liu, J.L.; *et al*. Probabilistic-constrained reliable H_∞ tracking control for a class of stochastic nonlinear systems: An outlier-resistant event-triggered scheme. J. Franklin Inst., **2021**, *358*: 4741−4760. doi: 10.1016/j.jfranklin.2021.04.012
35. Zou, L.; Wang, Z.D.; Geng, H.; *et al*. Set-membership filtering subject to impulsive measurement outliers: A recursive algorithm. IEEE/CAA J. Autom. Sin., **2021**, *8*: 377−388. doi: 10.1109/JAS.2021.1003826
36. Liu, Q.Y.; Wang, Z.D.; He, X.; *et al*. Event-based recursive distributed filtering over wireless sensor networks. IEEE Trans. Automat. Control, **2015**, *60*: 2470−2475. doi: 10.1109/TAC.2015.2390554
37. Wen, C.B.; Wang, Z.D.; Geng, T.; *et al*. Event-based distributed recursive filtering for state-saturated systems with redundant channels. Inf. Fus., **2018**, *39*: 96−107. doi: 10.1016/j.inffus.2017.04.004
38. Li, Q.; Wang, Z.D.; Li, N.; *et al*. A dynamic event-triggered approach to recursive filtering for complex networks with switching topologies subject to random sensor failures. IEEE Trans. Neural Netw. Learn. Syst., **2020**, *31*: 4381−4388. doi: 10.1109/TNNLS.2019.2951948

Citation: Bai, X.; Li, G.; Ding, M.; *et al*. Recursive Strong Tracking Filtering for Power Harmonic Detection With Outliers-Resistant Event-Triggered Mechanism. *International Journal of Network Dynamics and Intelligence*. 2024, 3(4), 100023. doi: 10.53941/ijndi.2024.100023